Volume 1 | Number 1 | Jan 2013 | Pages 1–100

PCCP

Physical Chemistry Chemical Physics
www.rsc.org/pccp

ROYAL SOCIETY OF CHEMISTRY

ROYAL SOCIETY OF CHEMISTRY

www.rsc.org/pccp

Journal Name

ARTICLE

TiO$_2$ (B) nanoparticles-functionalized WO$_3$ nanorods with enhanced gas sensing properties

Hongxin Zhang, Shurong Wang,* Yanshuang Wang, Jiedi Yang, Xueling Gao and Liwei Wang

In this work, TiO$_2$ (B) nanoparticles (NPs)-functionalized WO$_3$ nanorods (NRs) were first synthesized by a two-step solution strategy with a hydrothermal process for WO$_3$ NRs and a hydrolyzation process of Ti(OBu)$_4$ for the functionalization of TiO$_2$ (B) NPs. Various techniques, including SEM, TEM, XRD, and XPS, were employed to investigate the morphology, microstructure, crystalline nature and chemical composition of the prepared TiO$_2$ (B) NPs-functionalized WO$_3$ NRs. SEM and TEM results displayed that the TiO$_2$ (B)/WO$_3$ composite showed the rod-like nanostructure with a diameter range from 93 to 154 nm and a tough surface, which could increase the accessible surface area and the amount of surface active sites, thus improving the properties or performances of the as-prepared composite NRs. XRD and XPS analysis clearly verified that monoclinic TiO$_2$ (B) NPs, a metastable polymorph of TiO$_2$, were successfully supported on the WO$_3$ NRs. The gas sensing measurement results to several common reductive organic gases such as acetone, ethanol, ether, methanol and formaldehyde demonstrated that the sensor based on the as-obtained TiO$_2$ (B) NPs-functionalized WO$_3$ NRs exhibited obviously enhanced response compared with the pure WO$_3$ NR based sensor as well as fast response/recovery speed, good reproducibility and good stability, indicating their promising application in gas sensor. The excellent gas sensing performances should be contributed to the unique 1D rod-like nanostructure with tough surface, the existence of TiO$_2$-WO$_3$ heterojunctions and catalytic effect of the TiO$_2$ (B) NPs. The as-prepared TiO$_2$ (B) NPs-functionalized WO$_3$ NRs will have also a very good application prospect in electrochromic devices and catalysis.

Introduction

One-dimensional (1D) transition metal oxide nanostructures (nanotubes, nanowires, nanorods and nanobelts) have been studied extensively due to their unique chemical and physical properties resulted from the limited electron's motion in the confined dimensions and large surface-to-volume ratios.[1,2] Among the numerous transition metal oxides, tungsten oxide (WO$_3$), an indirect band gap n-type semiconductor, has attracted considerable attention due to its wide spectrum of potential applications.[3] In recent years, various 1D WO$_3$ nanostructured materials have been investigated for their applications in field emitters,[4,5] gas sensors,[6-8] electrochromic devices,[9,10] solar energy cells,[11] lithium-ion batteries,[12] electrocatalysis,[13] photocatalysis,[14] and water treatment.[15] Especially, it has been found that 1D WO$_3$ nanostructures with high crystallinity and high surface-to-volume ratio are good candidates for gas sensing materials in detecting some harmful gases such as NO$_2$[6,7] and NH$_3$[7] for the purpose of human health and environmental protection.

However, pure WO$_3$ nanomaterials are usually not efficient gas sensing materials because of low sensitivity and slow response/recovery speed and thus restrict their large scale industrial applications. Therefore, for effectively detecting toxic

and hazardous gases, significant efforts have been focused on improving the gas-sensing performance of WO$_3$ based gas sensors. It has been demonstrated that constructing WO$_3$ based nanocomposites is an effective method for enhanced gas sensing performances. For example, Zhu et al.[16] found that Pt-coated WO$_3$ (Pt-WO$_3$) nanowire film based sensor showed large electrical response to H$_2$ at room temperature. An et al.[17] prepared WO$_3$ nanorods/3.5 wt% graphene nanocomposites through a one-step hydrothermal method and found their superior sensitivity and selectivity to NO$_2$ gas. Bao et al.[18] reported that the gas sensing properties towards NO$_2$ could be enhanced by adding NiO to WO$_3$ based gas sensing material. Zhu et al.[19] fabricated TiO$_2$ (anatase)/WO$_3$ nanocomposites by a coprecipitation hydrothermal route using Na$_2$WO$_4$ as the W precursor and TiCl$_4$ as the Ti source and precipitator, and demonstrated that the TiO$_2$(anatase)/WO$_3$ nanocomposites showed good gas sensing properties for detecting vapors of benzene compounds.

Titanium dioxide (TiO$_2$), another important transition metal oxide, has been widely studied for its promising applications such as solar cells, photocatalysis, catalyst supports, water-splitting devices, antifogging and self-cleaning devices and sensors.[20] Generally, synthetic TiO$_2$ is obtained in three main crystal phases, namely anatase, rutile, and brookite. To date, besides enhanced gas sensing properties, TiO$_2$ (anatase or

rutile)/WO$_3$ nanocomposites have also been reported for the improved photocatalytic[21-23] and electrochromic[24-26] properties. Different from the common polymorphs of TiO$_2$, TiO$_2$(B), a metastable polymorph of TiO$_2$, has a less symmetrical monoclinic structure and was first obtained in 1980.[27] Recently, TiO$_2$ (B) has been demonstrated to have unique and enhanced electrochemical and catalytic properties, due to its metastable structural features and the lower thermodynamic stability of the crystal compared with other polymorphs of TiO$_2$.[28] However, to the best of our knowledge, there are few reports focused on the TiO$_2$ (B)/WO$_3$ nanocomposites. It should be expected that the TiO$_2$ (B) nanoparticles (NPs)-functionalized WO$_3$ nanorods (NRs) will have a very good application prospect in gas sensor, electrochromic devices and catalysis.

In the present study, TiO$_2$ (B) NPs-functionalized WO$_3$ NRs were first synthesized by a two-step solution process. The morphology, microstructure, crystalline nature and chemical composition of the obtained product were characterized in detail by means of SEM, TEM, XRD, and XPS techniques. The results clearly displayed that the TiO$_2$(B)/WO$_3$ composite had the rod-like nanostructure and a tough surface, and also verified that monoclinic TiO$_2$ (B) NPs were successfully supported on the WO$_3$ NRs. The as-prepared TiO$_2$ (B) NPs-functionalized WO$_3$ NRs were further employed to fabricate a gas sensor to detect several common reductive organic polluting gases including acetone, ethanol, ether, methanol and formaldehyde. The excellent gas sensing performances including high response, fast response/recovery speed, good reproducibility and good stability implied TiO$_2$ (B) NPs-functionalized WO$_3$ NRs' promising application in gas sensor. The TiO$_2$ (B) NPs-functionalized WO$_3$ NRs may also provide a potential opportunity to exploit other applications such as electrochromic devices and catalysis.

Experimental

Materials

Sodium tungstate dihydrate (Na$_2$WO$_4$•2H$_2$O) were purchased from Yingdaxigui Chemical Regent Company (Tianjin, China). Sodium chloride (NaCl), hydrochloric acid (HCl), tetrabutyl titanate (Ti(OBu)$_4$), absolute ethanol and toluene were obtained from Guangfu Fine Chemical Research Institute (Tianjin, China). All chemicals are of analytical grade (A.R.) and were used as received without further purification. Distilled water was used throughout the experiment.

Preparation of WO$_3$ NRs

WO$_3$ NRs were prepared by the reported simple one-pot hydrothermal method with NaCl as a capping agent with further modification.[9] Typically, 3.30 g of Na$_2$WO$_4$·2H$_2$O and 1.16 g of NaCl were dissolved in 75 mL of distilled water, and the pH value of the solution was adjusted to 2.5 using 3 mol/L HCl aqueous solution. The above solution was transferred into a Teflon-lined stainless steel autoclave (100 mL) and maintained at 180°C for 24 h. After cooled down to room temperature naturally, the obtained white WO$_3$ nanorods were collected by centrifugation and washed several times with distilled water and absolute ethanol before dried at 80°C.

Preparation of TiO$_2$ (B) NPs-functionalized WO$_3$ NRs

For the preparation of TiO$_2$ (B) NPs-functionalized WO$_3$ NRs, 0.2 g of the above gained and milled WO$_3$ NRs were dispersed into 100 mL of mixed solution of distilled water and absolute ethanol with a volume ratio of 1:4, and was vigorously stirred for 30 min. 0.0947 g of Ti(OBu)$_4$ was dissolved in 100 mL of toluene, and then introduced drop-wise into aforementioned WO$_3$ solution. Afterwards, the mixture was placed in the 70°C water bath until evaporated. The gray precipitate was collected by centrifugation, washed with distilled water and absolute ethanol, dried at 80°C and calcined at 400°C for 1h to obtain TiO$_2$/WO$_3$ composite NRs.

Characterization

The morphology of the as-prepared samples was characterized by scanning electron microscope (SEM, Shimadzu SS-550, 15kV) and transmission electron microscope (TEM, Philips FEI Tecnai 20ST). X-ray diffraction (XRD) analysis was carried out using a Rigaku D/max-2500 diffractometer with Cu Kα (λ = 1.5418 Å). The electronic structure of the surface of samples was characterized by means of X-ray photoelectron spectroscopy (XPS, Kratos Axis Ultra DLD spectrometer, Al-Kα X-ray monochromator).
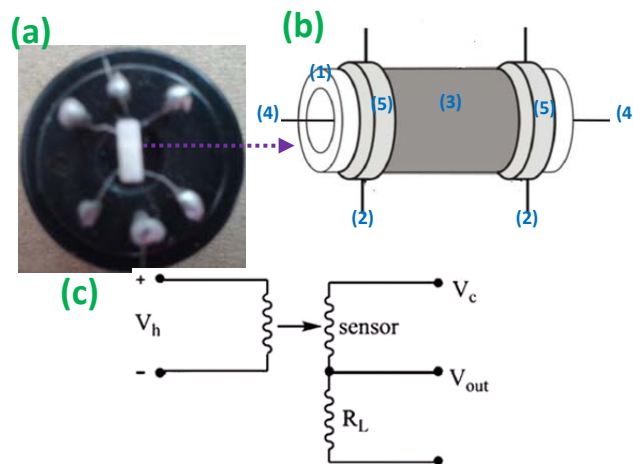
Fig. 1. (a) Photograph of the fabricated gas sensor unit, (b) construction of gas sensor [(1) Alumina tube, (2) Pt wire, (3) Sensing film, (4) Ni-Cr alloy heater, and (5) Au electrode], and (c) working principle of gas sensor test (V$_h$: Heating voltage; V$_{out}$: Output signal voltage; V$_c$: Test circuit voltage; R$_L$: Load resistance).

Gas sensing fabrication and tests

An appropriate amount of sample was mixed evenly with a couple of drops of distilled water to form slurry. Then the slurry was coated onto an alumina tube with a diameter of 1 mm and a length of 4 mm, which was positioned with two Au electrodes and four Pt wires on both end of the tube. A Ni–Cr alloy filament was put through the alumina tube and used as a heater by tuning the heating voltage. The alumina tube was then welded onto a six-probe pedestal to give the final gas sensor unit. The gas sensing tests were performed on a commercial WS-30A Gas-sensing Measurement System (Weisheng

Electronics Co., Ltd., Henan, China) at a relative humidity of about 30%, R_L = 4.7MΩ, V_c = 5V, using air as the dilution and reference gas. Target gases were introduced into the testing chamber on WS-30A microsyringe. The sensor response is defined as the ratio R_a/R_g, where R_a is the sensor resistance in air and R_g is the sensor resistance in the mixed gas of the tested gas and air, respectively. Fig. 1 shows the fabricated gas sensor unit, construction of gas sensor and the working principle of the gas sensing measurement system.

Results and discussion

Preparation and Characterization

TiO_2 NPs-functionalized WO_3 NRs were prepared in two steps. In the first step, Na_2WO_4 was converted into H_2WO_4 in the presence of excess hydrochloric acid (Eq. (1) , and then the H_2WO_4 precursors decomposed into WO_3 nanocrystals (Eq. (2)), which oriented grew into 1D WO_3 NRs under the hydrothermal condition of 180°C, with NaCl as the capping agent.[9] In the second step, the obtained WO_3 NRs were used as supports to load TiO_2 NPs via the following process, as illustrated in Fig. 2. To begin with, $TiO_2 \cdot nH_2O$ NPs were gradually formed by the hydrolyzation of $Ti(OBu)_4$ according to the Eq. (3). The generated $TiO_2 \cdot nH_2O$ NPs linked with WO_3 NRs through the hydrogen bonding effect. After that, TiO_2 NPs were produced and attached on the surface of the WO_3 NRs by the calcination treatment of 400°C (Eq. (4)).

$$Na_2WO_4 + 2HCl \rightarrow H_2WO_4 + 2NaCl \quad (1)$$

$$H_2WO_4 \rightarrow WO_3 + H_2O \quad (2)$$

$$Ti(OBu)_4 + (n+2)H_2O \rightarrow TiO_2 \cdot nH_2O + 4HOBu \quad (3)$$

$$TiO_2 \cdot nH_2O \rightarrow TiO_2 + nH_2O \quad (4)$$
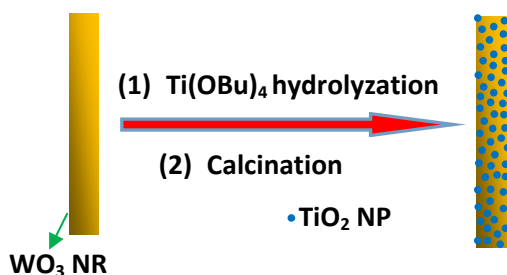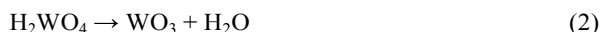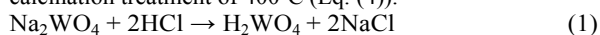
Fig. 2 Schematic illustration of the formation process for the TiO_2 NPs-functionalized WO_3 NRs.

The morphology and microstructure of the obtained pure WO_3 NRs and TiO_2 NPs-functionalized WO_3 NRs were investigated by SEM and TEM. Fig. 3a gives a representative low-magnification SEM image of as-synthesized WO_3 NRs, showing that the WO_3 sample presents an overall rod-like structure. It can be seen from the high-magnification SEM in Fig. 3b that these NRs have a diameter range from 93 to 154 nm. Fig. 3c and d show the SEM images of TiO_2 NPs-functionalized WO_3 NRs. As shown, the rod-like nanostructures are well retained, and the sizes of the NRs are almost not changed, which reveals that the morphology and structure of the samples can be kept after WO_3 NRs were functionalized by TiO_2 NPs. More detail of morphological and structural features was studied using TEM. The typical TEM image in Fig. 4a clearly displays the rod-like structure of the as prepared TiO_2/WO_3 nanocomposites. It can be observed from the high-magnification

TEM image in Fig. 4b that the surface of the composite NRs is very coarse, which can dramatically increase the accessible surface area and the amount of surface active sites, thus improving the properties or performances of the as-prepared NRs. It is not easy to clearly distinguish TiO_2 NPs in the performed TiO_2/WO_3 composite, indicating that ultrathin TiO_2 NPs were obtained and highly dispersed on the surface of the WO_3 NRs, which is consistent with the following XRD analysis results.
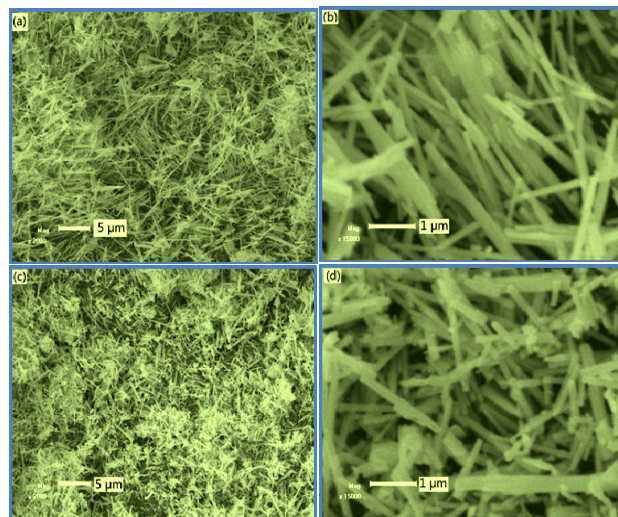
Fig. 3 SEM images of (a, b) the pure WO_3 NRs and (c, d) TiO_2 NPs-functionalized WO_3 NRs.
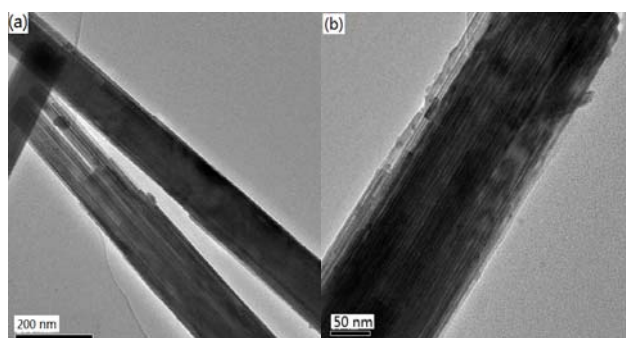
Fig. 4 (a) Low-magnification and (b) high-magnification TEM images of as-prepared TiO_2 NPs-functionalized WO_3 NRs.

In order to confirm the crystalline nature and composition of as-prepared WO_3 NRs and TiO_2 NRs-functionalized WO_3 NRs, XRD analysis was carried out. Fig. 5a shows the XRD pattern of the pure WO_3 NRs. All diffraction peaks can be well indexed to the corresponding planes of hexagonal WO_3 structure [space group P6/mmm (191)] with cell parameters of a = b = 7.30 Å, and c = 3.90 Å (JCPDS card No. 33-1387), and no other additional impurity peaks such as $WO_3 \cdot H_2O$ and WO_{3-x} ($0 < x \leq 3$) are detected, which suggests the high purity of the as-synthesized WO_3 NRs. These peaks are strong and narrow, indicating good crystallinity of the as-prepared WO_3 NRs. For the XRD pattern of TiO_2 NPs-functionalized WO_3 NRs, as shown in Fig. 5b, in addition to the main diffraction peaks related to hexagonal WO_3 phase , three new diffraction peaks at 2θ = 15.18, 29.82 and 35.38° are also clearly observed, and they correspond to the d-spacing values of 5.83, 2.98,

and 2.54 nm, respectively, which are perfectly indexed to monoclinic TiO_2 (B) crystal phase [space group C2/m (12)] with lattice cell parameters of a = 12.21 Å, b = 3.75 Å, and c = 6.54 Å (JCPDS card No. 46-1238). The obvious broadening of these diffraction peaks indicates that the obtained TiO_2 particles are nanocrystals with a small size. The XRD analysis result well demonstrates that the monoclinic TiO_2 (B) NPs were successfully supported on the WO_3 NRs.
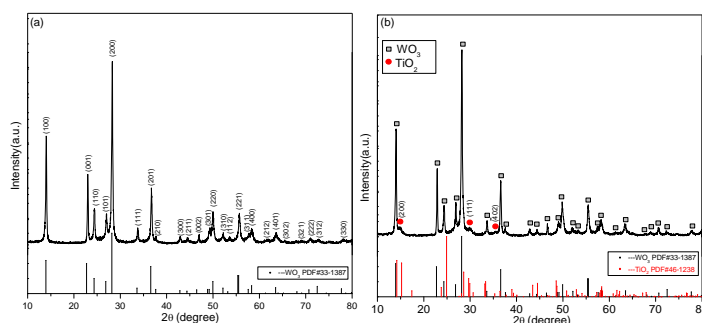
Fig. 5 XRD patterns of (a) the pure WO_3 NRs and (b) TiO_2 NPs-functionalized WO_3 NRs.
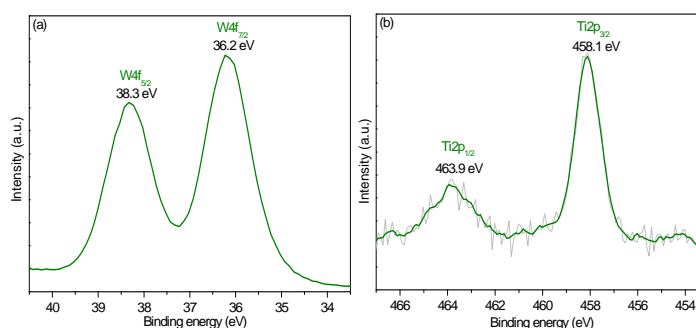
Fig. 6 XPS of the TiO_2 NPs-functionalized WO_3 NRs: (a) W 4f, and (b) Ti 2p.

To further verify TiO_2 NPs supported on the WO_3 NRs, the surface chemical component of TiO_2/WO_3 composite is detected by the XPS technique, which is often applied to analyze elements and atomic concentration and identify their corresponding valance state. Fig. 6 (a) and (b) show the high-resolution XPS spectra for W 4f and Ti 2p, respectively. In Fig. 6a, the binding energy (BE) of W $4f_{5/2}$ and W $4f_{7/2}$ are determined to be 38.3 V and 36.2 eV, respectively, and the splitting of the 4f doublet is 2.1 eV, which can be inferred the 6+ oxidation valence state of W. The W 4f peaks of the as prepared WO_3 NRs show a stoichiometric feature of WO_3, and the result of XPS experiment is consistent with the reported references.[30,31] The Ti 2p spectrum (Fig. 6b) comprises two symmetrical peaks with BEs of 463.9 eV and 458.1eV, which are attributable to Ti $2p_{1/2}$ and Ti $2p_{3/2}$, respectively, indicating the existence of a Ti (IV) oxidation state in the product.[32, 33] The molar content of TiO_2 is determined by XPS to be 11.03 mol. %. The above XPS results confirm that TiO_2 has been successfully supported on the surface of the WO_3 NRs.

Gas sensing properties

To investigate the gas sensor application of the as-fabricated TiO_2 NPs-functionalized WO_3 NRs, the gas sensing behavior measurement was performed towards several common reductive

organic polluting gases such as acetone, ethanol, ether, methanol and formaldehyde.
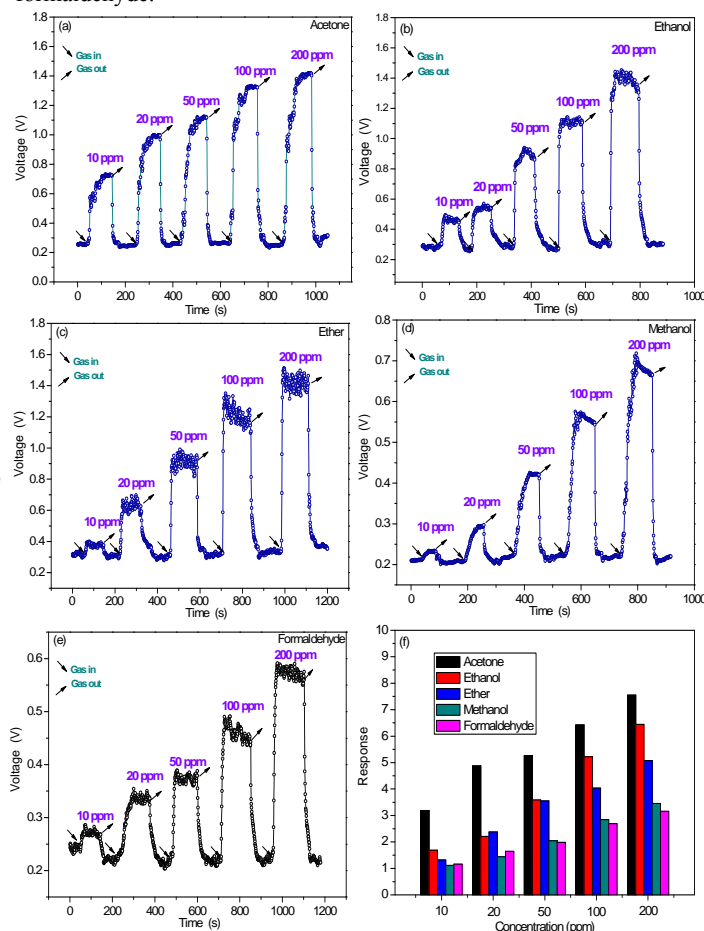
Fig. 7 Dynamic response-recovery curves of the sensor based on the TiO_2 NPs-functionalized WO_3 NRs to different concentrations of tested gases: (a) acetone, (b) ethanol, (c) ether, (d) methanol and (e) formaldehyde. (f) The corresponding responses.

Fig.7 (a-f) show the dynamic response-recovery curves and the corresponding responses of the sensor based on the TiO_2 NPs-functionalized WO_3 NRs upon exposure to the five kinds of gases with different concentrations (10, 20, 50, 100, and 200 ppm), respectively. From these dynamic response-recovery curves shown in Fig. 7 (a-e), it can be clearly observed that the output signal voltage of the sensor increases dramatically on the injection of these reductive gases, then decreases and recovers to the initial value after these gases are released, indicating the n-type response of the TiO_2 NPs-functionalized WO_3 NR based sensor. It can also be seen that the response amplitudes of the sensor are increased with increasing the tested gas concentration, and the sensor shows remarkable signal change upon exposure to low concentration (10 ppm) of reductive gases. For the practical application, in addition to the required high response amplitudes, a sensor should have short response/recovery times. The response time and recovery time is defined as the time for the sensor to reach 90 % of its maximum response and to fall to 10 % of its maximum response, respectively. These figures display that the sensor exhibits rapid response/recovery characteristics to the tested gases with average response time and recovery time of 25 and 11 s to acetone, 8 and 17 s to ethanol, 8 and 16 s to ether, 28 and 12 s to methanol, and 30 and 10 s to formaldehyde, respectively. The

short response and recovery times less than 30 s could be explained by the structure of 1D NRs for the gas sensing reaction, which is an apparent and common feature for all 1D nanostructure sensors.[34] The 1D rod-like structure can facilitate fast mass transfer of the tested gas molecules from the interaction region and also improve the rate for charge carriers to traverse the barriers induced by molecular recognition along the rods.[35-37] Such fast response and recovery speeds are convenient when the sensor is required to continuously detect the target gases. Fig. 7f presents the corresponding responses versus various gas concentrations (10-200 ppm) for the TiO_2 NPs-functionalized WO_3 NR based gas sensor. It can be seen that the sensor shows high response to these reductive gases, and the sensor responses to all the tested gases increase as increasing gas concentration, with the highest response of 7.6 to 200 ppm of acetone, 6.4 to 200 ppm of ethanol, 5.1 to 200 ppm of ether, 3.5 to 200 ppm of methanol, and 3.2 to 200 ppm of formaldehyde.
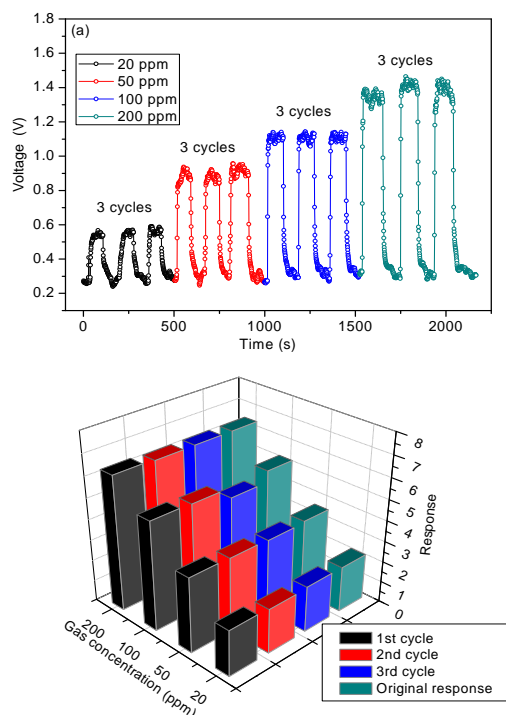
Fig. 8 (a) Dynamic response-recovery curves and (b) corresponding responses of the sensor based on the TiO_2 NPs-functionalized WO_3 NRs for different concentrations of ethanol (with 3 cycles) after 3 months.

Reproducibility and stability are another two important factors that must be considered as being acceptable if a gas sensor is to be utilized for reliable applications. Taking ethanol for example, the reproducibility and stability measurement of the TiO_2 NPs-functionalized WO_3 NR based sensor was carried out after three months. Fig. 8 (a) and (b) reveal the dynamic response-recovery curves and corresponding responses of the sensor based on the TiO_2 NPs-functionalized WO_3 NRs for different concentrations of ethanol with three repeated cycles after three months. As shown in Fig. 8a, to four tested ethanol concentrations, the sensor can maintain its initial response amplitude without a clear decrease upon three successive sensing tests to same concentration of ethanol, implying a good reproducibility of the as-fabricated TiO_2 NPs-functionalized WO_3 NR based sensor. Fig. 8b displays the corresponding sensor response to four ppm levels of ethanol over three repeated cycles

together with the original response to ethanol. It is clear that the TiO_2 NPs-functionalized WO_3 NR based gas sensor presents still high response and compared with the original response value, to all the same concentrations of ethanol, the sensor only shows a slight deviation of response value, which reveals a good stability and reproducibility of the fabricated sensor.
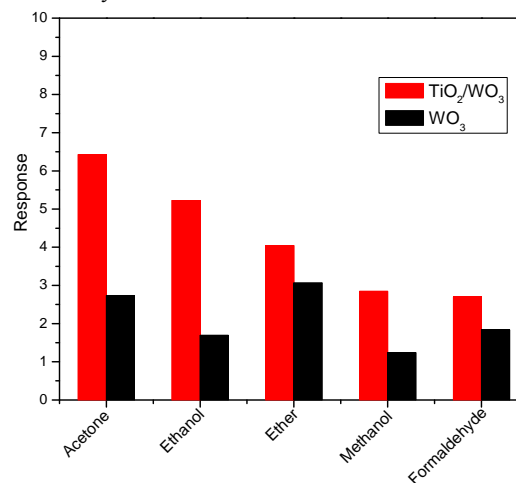
Fig. 9 Response comparison of the sensors based on the pure WO_3 NRs and the TiO_2/WO_3 composite NRs towards 100 ppm of various tested gases.

Fig. 9 displays the response comparison of the sensor based on pure and TiO_2 NPs-functionalized WO_3 NRs. It is clearly that compared with the pure WO_3 sensor, the sensor based on TiO_2 NPs-functionalized WO_3 NRs exhibits significantly enhanced response to all the five tested gases, with the increased response of 2.3 times to acetone, 3.1 times to ethanol, 1.3 times to ether, 2.3 times to methanol and 2.4 times to formaldehyde, respectively. Generally, gas sensing materials with a response higher than 2.0 can well meet the demand of commercial applications. It can be found from the figure that the pure WO_3 sensor shows very low response to ethanol (1.7), methanol (1.24) and formaldehyde (1.8). Satisfactorily, after functionalized by TiO_2 NPs, the sensor shows a high response to ethanol (5.2), methanol (2.8) and formaldehyde (2.7), which can meet the demand of commercial applications. Meanwhile, the responses to acetone and ether are also raised to 6.4 and 4.0, respectively. Therefore, it should be suggested that the TiO_2 NPs-functionalized WO_3 NRs are very promising sensing materials for detecting these reductive organic gases.

Gas sensing mechanism

WO_3 is an n-type semiconductor, thus its sensing mechanism generally can be interpreted by the classical electron depletion theory.[38,39] At a proper operating temperature, when WO_3 NRs are exposed to air, the oxygen molecules adsorbed on the surface of WO_3 NRs can capture electrons from the conduction band of WO_3 NRs to form the adsorbed oxygen ions ($O^{\delta-}$: O^{2-}, O^- and O_2^-),[39] and thus the WO_3 NR sensor has an increased resistance, due to the formation of electron depletion layer on the surface region of WO_3 NRs.[40] When the WO_3 NRs are exposed to a reductive gas such as acetone, ethanol and ether, these gas molecules can be oxidized by the surface adsorbed oxygen ions and consequently, the depleted electrons will be released back to the conduction band of WO_3, leading to a decreased resistance. If the resistance change is obvious, the sensor can show response to the tested gases. Clearly, the amount

of adsorbed oxygen ions and the rate of sensing reaction on the surface are critical for the sensing performance of the sensor. In the present work, the unique 1D rod-like nanostructure and tough surface of the as-prepared TiO_2 NPs-functionalized WO_3 NRs can improve the accessible surface area and surface active sites, which can result in an increase in the amount of the surface adsorbed oxygen ions due to a higher surface-to-volume ratio and better electron mobility compared with conventional nanomaterial, quicken the rate of sensing reaction between reductive gases and the surface adsorbed oxygen ions, and facilitate the gas adsorption and diffusion on the composite NRs, thus leading to an enhanced gas sensing performance.
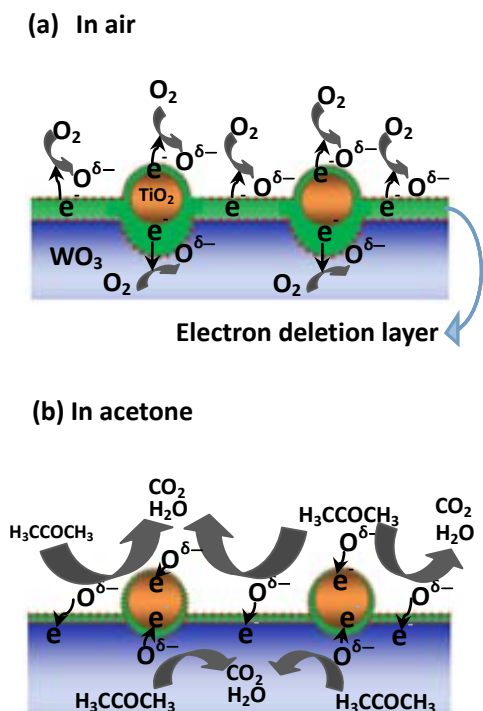
Fig. 10 Schematic diagram of the surface sensing reaction mechanism of reductive gases (taking acetone gas as an example) on TiO_2 NPs-functionalized WO_3 NR based sensor.

More importantly, because the sensing reactions happen on the surface of the WO_3 NRs, the surface functionalization of the WO_3 NRs by TiO_2 NPs will be expected to remarkably enhance the gas sensing performances. First of all, the existence of TiO_2-WO_3 heterojunctions makes a significant contribution to the enhanced gas sensing performance of the TiO_2 NPs-functionalized WO_3 NR based sensor.[41-43] Because TiO_2 and WO_3 have different band gaps and work functions, when TiO_2 NPs and WO_3 NRs contact each other, a heterojunction with a Schottky potential barrier will be formed at the interface between TiO_2 NPs and WO_3 NRs.[41-43] It should be noted that electron transport in the TiO_2 NPs-functionalized WO_3 NRs may be different from that of pure WO_3 NRs because of the formation of heterojunctions at the interfaces of TiO_2/WO_3, which will result in the enhanced conductance modulation.[44] As illustrated in Fig. 10a, when the TiO_2 NPs-functionalized WO_3 NRs is exposed to air, compared with the pure WO_3 NRs, a thicker electron depletion layer will be formed on the surface region of the TiO_2 NPs and WO_3 NRs, and an additional electron depletion region is also formed at the interfaces of TiO_2/WO_3, which facilitates the dissociation of molecular oxygen. Besides, TiO_2(B) NPs also significantly increase the quantity of active adsorbed oxygen ions through the catalytic

dissociation of molecular oxygen,[45] which also results in a stronger degree of electron depletion on the WO_3 surface region and higher sensitivity compared with the pure WO_3. When the sensor is exposed to the reductive gas such as acetone, the acetone molecules will be allowed to react with more adsorbed oxygen ions to produce CO_2 and H_2O, and more trapped electrons can pass through the TiO_2/WO_3 interfaces and return to the conduction band of the WO_3 NRs (Fig. 10b), which leads to lower sensor resistance and improved sensor response.

Conclusions

In summary, TiO_2 (B) NPs-functionalized WO_3NRs were first synthesized by a two-step solution strategy, and characterized by various techniques. The gas sensing behavior was investigated in detail to several common reductive organic gases including acetone, ethanol, ether, methanol and formaldehyde. The results revealed that the sensor based on the as-prepared TiO_2 (B) NPs-functionalized WO_3 NRs exhibited remarkably enhanced response compared with the pure WO_3 NR based sensor together with quick response/recovery characteristics, good reproducibility and good stability, indicating their promising application as gas sensing materials. The enhanced gas sensing performances can be contributed to the unique 1D rod-like nanostructures with a tough surface, the existence of TiO_2-WO_3 heterojunctions at the interferes of TiO_2 NPs/WO_3 NRs and catalytic effect of the TiO_2 (B) NPs. The as-obtained TiO_2 (B) NPs-functionalized WO_3 NRs will have also potential applications in other fields such as electrochromic devices and catalysis.

Notes and references

* Tianjin Key Lab of Metal and Molecule-based Material Chemistry, Department of Chemistry, Nankai University, Tianjin, 300071, China.

Fax: +86–22–23502458;

Tel: +86–22–23505896;

E-mail: shrwang@nankai.edu.cn

1 F. C. Cheong, B. Varghese, Y. W. Zhu, E. P. S. Tan, L. Dai, V. B. C. Tan, C. T. Lim and C. H. Sow, *J. Phys. Chem. C,* 2007, **111**, 17193-17199.

2 D. Banerjee, S. H. Jo, Z. F. Ren, *Adv. Mater.*, 2004, **16**, 2028–2032.

3 F. Zheng, M. Guo and M. Zhang, *CrystEngComm*, 2013, **15**, 277–284.

4 L. Li, Y. Zhang, X. S. Fang, T. Y. Zhai, M. Y. Liao, X. L. Sun, Y. S. Koide, Y. S. Bando and D. Golberg, *J. Mater. Chem.*, 2011, **21**, 6525-6530.

5 F. Liu, L. Li, F. Y. Mo, J. Chen, S. Z. Deng and N. S. Xu, *Crystal Growth & Design*, 2010, **10**, 5193-5199.

6 S. L. Bai, K. W. Zhang, R. X. Luo, D. Q. Li, A. F. Chen and C. C. Liu, *J. Mater. Chem.*, 2012, **22**, 12643-12650.

7 B. B. Cao, J. J. Chen, X. J. Tang and W. L. Zhou, *J. Mater. Chem.*, 2009, **19**, 2323–2327.

8 G. Wang, Y. Ji, X. R. Huang, X. Q. Yang, P. -I. Gouma and M. Dudley, *J. Phys. Chem. B*, 2006, **110**, 23777-23782.

9 J. M. Wang, E. Khoo, P. S. Lee and J. Ma, *J. Phys. Chem. C*, 2009, **113**, 9655–9658.

10 J. Zhang, J. P. Tu, X. H. Xia, X. L. Wang and C. D. Gu, *J. Mater. Chem.*, 2011, **21**, 5492–5498.

11 K. Hara, Z. G. Zhao, Y. Cui, M. Miyauchi, M. Miyashita and S. Mori, *Langmuir* 2011, **27**, 12730–12736.

12 L. N. Gao, X. F. Wang, Z. Xie, W. F. Song, L. J. Wang, X. Wu, F. Y. Qu, D. Chen and G. Z. Shen, *J. Mater. Chem. A*, 2013, **1**, 7167–7173.

13 A. Phuruangrat, D. J. Ham, S. J. Hong, S. Thongtem and J. S. Lee, *J. Mater. Chem.*, 2010, **20**, 1683–1690.

14 Z. G. Zhao and M. Miyauchi, *Angew. Chem., Int. Ed.*, 2008, **47**, 7051–7055.

15 J. Li, X. H. Liu, Q. F. Han, X. X. Yao and X. Wang, *J. Mater. Chem. A*, 2013, **1**, 1246-1253.

16 L. F. Zhu, J. C. She, J. Y. Luo, S. Z. Deng, J. Chen and N. S. Xu, *J. Phys. Chem. C*, 2010, **114**, 15504–15509.

17 X. Q. An, J. C. Yu, Y. Wang, Y. M. Hu, X. L. Yu and G. J. Zhang, *J. Mater. Chem.*, 2012, **22**, 8525-8531.

18 M. Bao, Y. J. Chen, F. Li, J. M. Ma, T. Lv, Y. J. Tang, L. B. Chen, Z. Xu and T. H. Wang, *Nanoscale*, DOI: 10.1039/C3NR05268K.

19 Y. Zhu, X. T. Su, C. Yang, X. Q. Gao, F. Xiao and J. D. Wang, *J. Mater. Chem.*, 2012, **22**, 13914–13917.

20 W. J. Liu, J. G. Wang, W. Li, X. J. Guo, L. H. Lu, X. H. Lu, X. Feng, C. Liu and Z. H. Yang, *Phys. Chem. Chem. Phys.*, 2010, **12**, 8721–8727.

21 D. Su, J. Y. Wang, Y. P. Tang, C. Liu, L. F. Liu and X. J. Han, *Chem. Commun.*, 2011, **47**, 4231–4233.

22 L. Zhang, Y. G. Li, Q. H. Zhang and H. Z. Wang, *CrystEngComm*, 2013, **15**, 5986–5993.

23 X. B. Luo, F. Deng, L. J. Min, S. L. Luo, B. Guo, G. S. Zeng and C. Au, *Environ. Sci. Technol.*, 2013, **47**, 7404−7412.

24 N. M. Vuong, D. Kim and H. Kim, *J. Mater. Chem. C*, 2013, **1**, 3399–3407.

25 P. J. Wojcik, A. S. Cruz, L. Santos, L. Pereira, R. Martins and E. Fortunato, *J. Mater. Chem.*, 2012, **22**, 13268–13278.

26 Y. -C. Nah, A. Ghicov, D. Kim, S. Berger and P. Schmuki, *J. AM. CHEM. SOC.*, 2008, **130**, 16154–16155.

27 R. Marchand, L. Brohan and M. Tournoux, *Mater. Res. Bull.*, 1980, **15**, 1129-1133.

28 W. Sugimoto, O. Terabayashi, Y. Murakami and Y. Takasu, *J. Mater. Chem.*, 2002, **12**, 3814–3818.

29 Aravindan, N. Shubha, W. C. Ling and S. Madhavi, *J. Mater. Chem. A*, 2013, **1**, 6145–6151.

30 M. T. Chang, L. J. Chou, Y. L. Chueh, Y. C. Lee, C. H. Hsieh, C. D. Chen, Y. W. Lan and L. J. Chen, *Small*, 2007, **3**, 658-664.

31 R. S. Vemuri, K. K. Bharathi, S. K. Gullapalli and C. V. Ramana, *ACS Appl. Mater. Interfaces*, 2010, **2**, 2623-2628.

32 N. Ohtsu, N. Masahashi, Y. Mizukoshi and K. Wagatsuma, *Langmuir*, 2009, **25**, 11586–11591.

33 S. B. Amor, G. Baud, M. Benmalek, H. Dunlop, R. Frier and M. Jacquet, *J. Adhes.*, 1998, **65**, 307–329.

34 Y. J. Chen, C. L. Zhu, L. J. Wang, P. Gao, M. S. Cao and X. L. Shi, *Nanotechnology*, 2009, **20**, 045502-045507.

35 X. H. Liu, J. Zhang, X. Z. Guo, S. H. Wu and S. R. Wang, *Nanoscale*, 2010, **2**, 1178–1184.

36 L. W. Wang, Y. F. Kang, X. H. Liu, S. M. Zhang, W. P. Huang and S. R. Wang, *Sensors & Actuators: B*, 2012, **162**, 237–243.

37 L. W. Wang, S. R. Wang, M. J. Xu, X. J. Hu, H. X. Zhang, Y. S. Wang and W. P. Huang, *Phys. Chem. Chem. Phys.*, 2013, **15**, 17179-17186.

38 D. E. Williams, *Sens. Actuators B: Chem*, 1999, **57**, 1–16.

39 N. Barsan and U. J. Weimar, *J. Electroceram.*, 2001, **7**, 143–167.

40 N. J. Dayan, S. R. Sainkar and R. N. Karekar, R. C. Aiyer, *Thin Solid Films*, 1998, **325**, 254-258.

41 J. Zhang, X. H. Liu, L. W. Wang, T. L. Yang, X. Z. Guo, S. H. Wu, S. R. Wang and S. M. Zhang, *Nanotechnology*, 2011, **22**, 185501-185507.

42 H. Zhang, R. Wu, Z. Chen, G. Liu and Z. Zhang, *CryEngComm*, 2012, **14**, 1775-1782.

43 J. Huang, X. Xu, C. Gu, M. Yang and M. Yang, *J. Mater. Chem.*, 2011, **21**, 13283-13289.

44 D. Bekermann, A. Gasparotto, D. Barreca, C. Maccato, E. Comini, C. Sada, G. Sberveglieri, A. Devi and R. A.Fischer, *ACS Appl. Mater. Interfaces*, 2012, **4**, 928−934.

45 C. C. Li, L. M. Li, Z. F. Du, H. C. Yu, Y. Y. Xiang, Y. Li, Y. Cai and T. H. Wang, *Nanotechnology*, 2008, **19**, 035501-035504.